arXiv:0902.3015v1 [cond-mat.supr-con] 17 Feb 2009

Giant Nonlinear Electron-lattice Interaction in Cuprate Superconductors, and Origin of the Pseudogap

R. Nistor[2], G.J. Martyna[1], M. H. Müser[1,2], D.M. Newns[1], and C.C. Tsuei [1]

[1]*IBM T.J. Watson Research Center,*

Yorktown Heights, NY 10598, USA and

[2]*Dept. of Applied Mathematics, University of Western Ontario,*

London, Ontario, CANADA N6A 5B7

Abstract

The pseudogap is a key property of the cuprate superconductors, whose understanding should illuminate the pairing mechanism. Recent experimental data support a close connection between the pseudogap and an oxygen-driven C4 symmetry breaking within the CuO_2 plane unit cell. Using ab initio Molecular Dynamics, we demonstrate the existence of a strong nonlinear electron-oxygen vibrator coupling in two cuprates. In a mean field approach applied to this coupling within a model Hamiltonian, we derive a C4 splitting/pseudogap phase diagram in agreement with experiment - providing an explanation for the pseudogap phenomenon from first principles. The implications for superconductivity and the Fermi surface arc effect are discussed.

In 20 years no consensus has emerged on the mechanism for d-wave high temperature superconductivity (HTS) in cuprates or for their characteristic pseudogap (PG) [1]. Alternatives such as the electron-lattice coupling which mediates pairing in conventional superconductors [2], and purely electronic mechanisms [3, 4], have been widely discussed. A possibly decisive input comes from recent work [5, 6] showing a strong correlation between the occurrence of the PG in the underdoped region and the breaking of C4 symmetry (i.e. the a and b directions become nonequivalent) in the planar oxygen vibrational amplitudes. This observation points to the origin of the PG as a lattice instability, and is a very important clue - consistent with evidence such as the doping-dependent oxygen isotope shift [7, 8] and the HTS-induced softening in oxygen vibration frequency [9, 10] - that electron-lattice coupling is the mechanism for HTS. Paradoxically, *ab initio* calculations do not find a strong conventional *linear* electron-lattice coupling in the cuprates [11, 12], leading to the proposition that a primarily *nonlinear* coupling lies at the heart of HTS.

In this paper we use *ab initio* molecular dynamics (AIMD) to show that electron coupling to the vibrations of O in the CuO_2 plane is in fact very strong - but it is *second order* in the oxygen displacement, in contradiction with the assumptions underlying the earlier electron-lattice coupling work [11, 12]. To explain why the coupling should be second order, we argue from symmetry that the local effect on the electrons of a radial displacement of oxygen in the Cu-O-Cu bond should be independent of the displacement's sign, and hence second order in the O displacement. Based on this symmetry argument, two of us earlier put forward the Fluctuating Bond Model of HTS [13] which is empirically based on the idea of second order coupling, an idea which had been proposed earlier [14, 15, 16]. The FBM successfully predicted C4 symmetry breaking [13] and enabled superconducting properties such as d-wave symmetry [17] to be understood. Unlike conventional superconductivity, the FBM has not yet been parametrized from first principles, and here we show that the value of the FBM coupling energy does indeed have the value required in the FBM [13], validating its key assumption of a giant nonlinear electron-lattice coupling.

The technique of *ab initio* molecular dynamics (AIMD) [18] solves the ionic equations of motion on a Born-Oppenheimer potential energy surface obtained by solution of the many-electron Schrodinger equation in local density approximation, a technique well suited to the present problem in that it avoids the constraint of a linearized interaction. We start by applying AIMD to the C4 symmetry-breaking in two cuprates. First we consider the

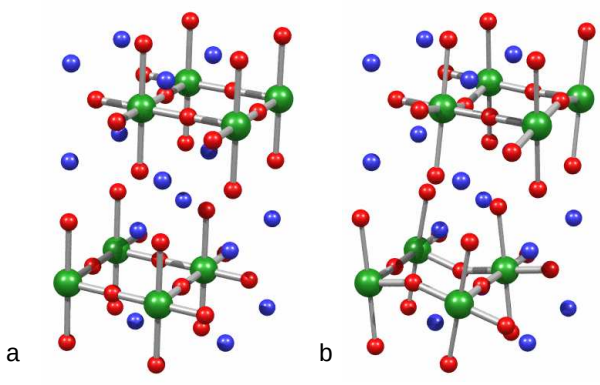

FIG. 1: *ab initio* Molecular Dynamics calculation at $T = 4\,\mathrm{K}$ of the structure of metallic La_2CuO_4 (214) [19], blue spheres, La, green spheres, Cu, red spheres, O. **a**, Undistorted setup structure, **b**, Equilibrated structure showing vertical displacements of the planar oxygens correspond to rotations of CuO_6 octahedra about alternate x- and y- axes in planes stacked along the c-axis - the LTT structure found at low temperature in metallic 214 phases.

well-established Low Temperature Tetragonal (LTT) structure [19] found in underdoped metallic 214 materials, which was early on linked to non-linear electron lattice coupling [20]. Figure 1 shows the LTT structure is predicted correctly by AIMD for the metallic La_2CuO_4 at $T = 4\,\mathrm{K}$. All CuO_2 planes undergo C4 symmetry-breaking in which one half of the oxygens undergo a z-displacement, the $\pi/2$ rotation of successive planes around the c-axis ensures overall tetragonal symmetry. The symmetry breaking by z-displacement in the 214 family contrasts with the symmetry breaking by xy-displacement in the 2212 and oxychloride ($Ca_2CuO_2Cl_2$) materials [6].

We now establish a model-independent global connection between oxygen PE surface and the number of electrons by extending the Fig. 1 type of calculation to a range of dopings. The oxychloride system $Ca_{2-x}Na_xCuO_2Cl_2$ is computationally attractive and doping can be controlled via the Na fraction x, the calculated oxygen PE surfaces being shown in Fig. 2. AIMD accurately reflects experiment [6] in that the oxygen displacemements are in the xy-plane (Fig. 2 inset) (but cannot capture its non-Born-Oppenheimer features). The PE surfaces in Fig. 2 are strongly dependent on doping, their minimum is off the bond axis (leading to the Fig. 2 inset distortion) at low doping, transitioning to an on-axis minimum

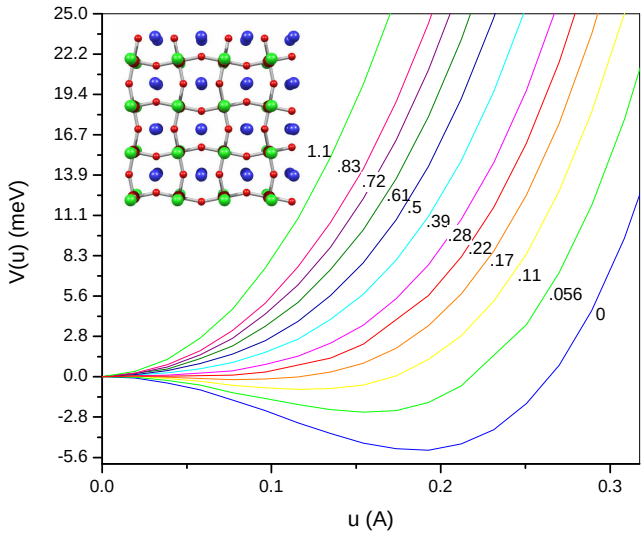

FIG. 2: PE curves $V(u)$ for oxychloride material as a function of oxygen in-plane distortion u (see insert) for different dopings (see labelling on curves). Doping is implemented by fractional substitution of Na for Ca.

(stability of oxygen on the bond axis) at high doping, and can be parametrized in the form

$$V(u) = (\chi + Vp)\,\frac{u^2}{2} + \frac{w}{8}u^4. \tag{1}$$

Here u is oxygen displacement from the bond axis, the zero-doping bond force constant χ is negative (oxygen unstable at zero doping), and the electron-lattice coupling V is positive, representing stabilization of the unstable Cu-O-Cu bond with increasing doping p. The positive quartic term w represents the confinement of oxygen in the local lattice cage. The results of Fig. 2 and Eq. (1) clearly show that the oxygen potential energy surface is strongly dependent on global electron number, with a coupling term in V going as the *square* of the oxygen displacement, as was argued above. If the Cu-O-Cu bond is sensitive to the global number of electrons, we can also anticipate a strong response of the oxygen to the *local* electron number.

To calculate the local form of electron-lattice coupling requires a model. We start from the Emery tight-binding model based on Cu $3d_{x^2-y^2}$ and the oxygen $2p_x/2p_y$ orbitals that have σ symmetry in the Cu-O-Cu bond. The coupling is determined by considering how the matrix elements vary with oxygen displacement, and projecting the result back into a

one-band basis of just the $3d_{x^2-y^2}$ orbitals (see Supp. Mat.). The resulting complete FBM Hamiltonian Eq. (2) is written in mixed representation electronically. It considers only one vibrational mode per oxygen for simplicity:

$$H = \sum_{\mathbf{k},\sigma} \epsilon_{\mathbf{k}} n_{\mathbf{k},\sigma} + \sum_{\langle i,j \rangle} \left[\frac{p_{ij}^2}{2M} + \frac{\chi_0}{2} u_{ij}^2 \right] + \frac{w}{8} \sum_{\langle i,j \rangle} u_{ij}^4 - \frac{v}{\sqrt{2}} \sum_{\langle i,j \rangle} N_{ij} u_{ij}^2. \quad (2)$$

Equation (2) embodies the conventional 1-band model [21] with a single $3d_{x^2-y^2}$ orbital per Cu atom located at site i in the CuO_2 plane. Here $c_{i,\sigma}^+$ ($c_{i,\sigma}$) is the creation (destruction) operator for the $3d_{x^2-y^2}$ orbital on site i of spin σ, with number operators $n_{i,\sigma} = c_{i,\sigma}^+ c_{i,\sigma}$, and $c_{\mathbf{k},\sigma}^+$ ($c_{\mathbf{k},\sigma}$) are the corresponding operators for the band states of wavevector $\mathbf{k}$, etc.. A sum over $\langle ij \rangle$ implies that each nearest-neighbor bond ij appears only once in the sum. The variables p_{ij}, u_{ij} are the conjugate momentum and position coordinates of oxygen in bond ij, M is oxygen mass and χ_0 the bare oxygen force constant. w is the quartic interaction, and v a (positive) electron-vibrator coupling constant. The operator $N_{ij} = \sum_\sigma \left(n_{i\sigma} + n_{j\sigma} - c_{i,\sigma}^+ c_{j,\sigma} - c_{j,\sigma}^+ c_{i,\sigma} \right)$ represents the number of electrons in the ij-antibonding orbital $\left[c_{i,\sigma} - c_{j,\sigma} \right] / \sqrt{2}$.

In more detail the first term of Eq.(2) is the electronic band energy, and the second term represents the harmonic part of the oxygen Hamiltonian, to which is added the third term, a quartic interaction which confines the oxygen and is needed to fit the PE curves in Fig 2. The nonlinear electron-vibrator coupling is represented in the fourth term, which involves the vibrator coordinate u_{ij} quadratically, and the electronic operator N_{ij}. Dumping electrons N_{ij} into the antibonding orbital in bond ij softens the vibrator ij, as implied by Eq. (1) and by the trend in Fig. 2 - it is also reasonable on intuitive chemical grounds. Note that the $c_{i,\sigma}^+ c_{j,\sigma} + c_{j,\sigma}^+ c_{i,\sigma}$ term in N_{ij}, which originates from processes where an electron hops from Cu i to O and then to Cu j, is identical to the original FBM [13], while the present analysis adds a new term $-\left(n_{i\sigma} + n_{j\sigma} \right)$, originating from processes where an electron hops from Cu to O and then ends up back on the same Cu.

The FBM coupling is strong between the oxygens and the saddle points at X= $(\pi, 0)$ and Y= $(0, \pi)$ in the band structure - the energies at X and Y are normally degenerate, but the degeneracy is split by C4 symmetry-breaking. The bare electron-lattice coupling constant v in Eq. (2) can be simply determined by displacing the x-oxygens and determining the

shift in the band structure eigenvalue at X. Any effect of a chemical potential shift can be removed by displacing the y-oxygens and subtracting the two effects (see Supp. Mat.). The results are collected in Table I for the 214 and oxychloride materials. The values of the quartic interaction w are obtained from the quartic coefficient of the fit to the Fig. 2 curves, and similar ones for the 214 material. It is found that the coupling v is relatively small for vibrational polarization along the Cu-O-Cu bond, so we only considered polarizations transverse to the bond in Table I.

Table I: FBM Parameters for 214 and Oxychloride Materials

Polarization	v_{214} (au)	v_{oxy} (au)	w_{214} (au)	w_{oxy} (au)
$xy \perp$ to bond	0.0163	0.0182	0.053	0.090
$z \perp$ to bond	0.0174	0.0202	0.122	0.106

Note that the coupling strengths v in Table I are rather material- and polarization-independent, while the anharmonic coefficents w vary by less than 2.5×.

The pairing energy in the FBM is second order in the coupling v, with the functional form [13] v^2/w. In the current form Eq.(2) it is $K' = 4v^2/w$ (see Supp. Mat.). From Table I K' can be estimated to be about $K' \simeq 0.5$ eV, matching the giant magnitude required [13] for high temperature superconductivity. This is the first meaningful *ab initio* prediction of the electron-lattice coupling constant in HTS, and points the way to an eventual quantitative theory of HTS by extending the existing body of work describing conventional superconductors.

Here, as an application of the model Eq.(2), rather than again presenting results for the gap equation [13] which will be done elsewhere, we present an important new result, the pseudogap phase diagram. This is done by the mean field decoupling of Eq.(2) (see Supp. Mat.), (a) $N_{ij}u_{ij}^2 \rightarrow \langle N_{ij}\rangle u_{ij}^2$, leading to a softening of the vibrator proportional to the number of antibonding electrons $\langle N_{ij}\rangle$, and (b) $N_{ij}u_{ij}^2 \rightarrow N_{ij}\left\langle u_{ij}^2\right\rangle$ wherein the nearest-neighbor hopping $\left(c_{i,\sigma}^{+}c_{j,\sigma} + c_{j,\sigma}^{+}c_{i,\sigma}\right)$ is reduced by increased vibrator amplitude $\left\langle u_{ij}^2\right\rangle$. In this mean field approximation the model decouples into exactly soluble band structure and anharmonic oscillator problems, linked by the mean field quantities $\langle N_{ij}\rangle$ and $\left\langle u_{ij}^2\right\rangle$, which are solved for self-consistently assuming they are uniform in space.

When the expectation values $\langle N_{ij}\rangle$ and $\left\langle u_{ij}^2\right\rangle$ in the x- and y-directed bonds are found to differ, C4 symmetry breaking in both *vibrator amplitudes* and the *electronic structure* occurs.

Symmetry breaking in the oxygen vibrator amplitudes is exactly the effect measured in the STM experiments of Ref. [6] (consistently we predict that the higher/lower-amplitude oxygens in the Ref. [6] R-plots should be dark/light streaks (see Supp. Mat.), as observed). C4 symmetry breaking in the electronic structure, wherein the degeneracy of the saddle points at X= $(\pi, 0)$ and Y= $(0, \pi)$ is split, leads to a d-type PG $\Delta_{ps}(\mathbf{k}) \sim \Delta_{ps}(\cos k_x - \cos k_y)/2$ (see Supp. Mat.), where the PG, Δ_{ps}, can be positive or negative in sign. The PG Δ_{ps} is one half the splitting between the energies at X and Y. The work of Ref. [5] shows that the experimental PG is intimately associated with the C4 splitting - confirming the correctness of identifying Δ_{ps} with the experimental pseudogap. The predicted PG phase diagram is shown in Fig. 3, and is seen to reproduce the known experimental phase diagram for the pseudogap [1, 5, 23, 24, 25]. At low temperature the pseudogap ranges from a maximum of about 100meV on the underdoped side, decreasing with increasing doping [5, 23, 24, 25, 26], while T^* behaves reasonably as a function of doping and is of the correct magnitude [1].

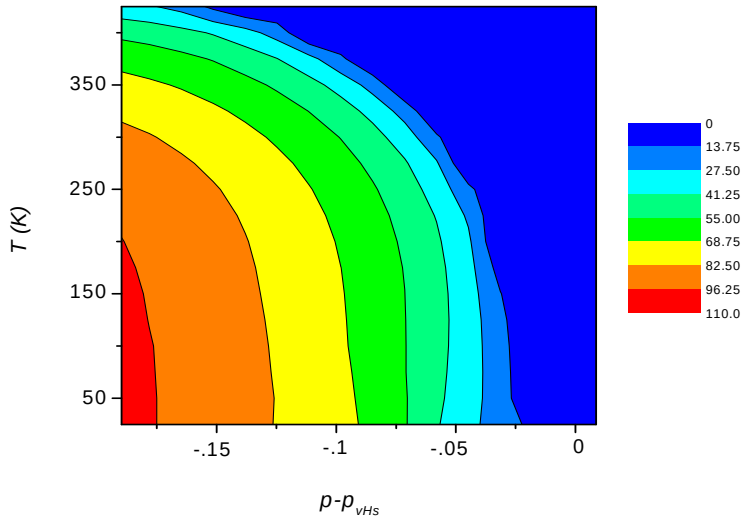

FIG. 3: Contour map of pseudogap in temperature/doping plane showing decrease with doping, and with temperature, until it vanishes at phase boundary T^*. Contours labelled by pseudogap Δ_{ps} in intervals of 13.75 meV. For experimental Δ_{ps} magnitudes see Ref. [26].

Note that experimentally, the C4 splitting is characterized by a nanoscale domain structure [6]. In our picture this implies that the sign of Δ_{ps} will vary spatially, in a manner such as $\Delta_{ps}(\mathbf{k}) \sim \cos\theta\Delta_{ps}(\cos k_x - \cos k_y)/2$, where θ is some local phase determined by the

local nanoscopic disorder. The Fermi surface in the C4 split phase will be sensitive to the sign of Δ_{ps}. The inset in Fig. 4 shows the two FS corresponding to the extreme cases $\theta = 0$ and $\theta = \pi$, and it is reasonable to assume that a nanoscopically varying order parameter will lead to FS smearing as illustrated by the shaded region in the Fig. 4 inset.

The smearing of the FS by the PG, seen in the Fig. 4 inset, is seen to be least near the nodal line $k_x = k_y$, a manifestation of the d-type nature of the PG $\Delta_{ps}(\mathbf{k})$, and to increase as one goes towards the SP's at X and Y. If we make a measurement on some energy scale E, it might be expected that the FS will be well-defined at $\mathbf{k}$-points where the local PG is less than E, $\Delta_{ps}(\mathbf{k}) < E$, but that it will appear smeared out on energy scales where the local PG is larger than E, $\Delta_{ps}(\mathbf{k}) > E$. As an example of this phenomenon we could take E to be temperature, $E = k_{\mathrm{B}}T$. According to this argument, there should then be a boundary between the resolvable and unresolvable sections of the FS arc defined by $\Delta_{ps}(\mathbf{k}) = k_{\mathrm{B}}T$. In fact this FS arc effect [27] has already been observed a couple of years ago, as shown by a comparison of the data with our heuristic model in Fig. 4, which is in good agreement with experiment [28] (this approach does not include the temperature-dependent quasiparticle lifetime broadening [27], which we hope to derive in a future paper dealing with quasiparticle dynamics).

The approach here has been to focus on the electron-lattice interaction while ignoring the strong electron correlation effects. It would be productive to consider the nonlinear electron-lattice coupling in the context of a strongly correlated (large-U) system, where the modulation of the Cu-Cu bond by oxygen vibration is expected to be as strong as in the noninteracting case, and the phase diagram can be extended to include magnetic effects.

In conclusion, using AIMD we have demonstrated the instability of the CuO_2 plane oxygens in three cuprates which relates closely to experiments such as the LTT structure in the 214 family and the C4 symmetry breaking in the 2212 and oxychloride materials. The nonlinear electron-lattice coupling deduced from these calculations is large with the magnitude required by the FBM theory. Using our deduced Hamiltonian Eq. (2), we are able to derive the pseudogap phase diagram, harmonizing the pseudogap data with the observed C4 splitting, and to understand the temperature-dependent Fermi arc observations.

---

[1] T. Timusk et al., Rep. Prog. Phys. **62,** 61 (1999).

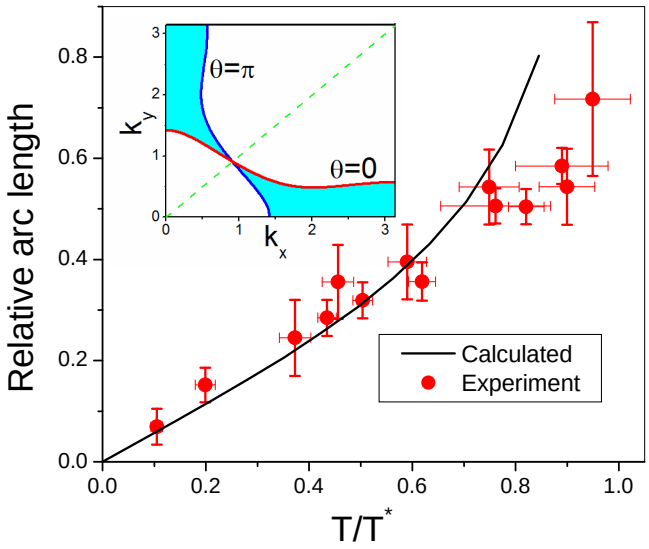

FIG. 4: Inset: two FS's for domains with opposite sign of pseudogsap (Δ_{ps} = 74 meV), colored area indicates approximate loss of definition of FS in a nanoscopically disordered sample. Plot of FS arc length vs. temperature compared with experiment (see text).

[2] E.G. Maksimov, M.L. Kuli´c, and O.V. Dolgov, arXiv:0810.3789 [cond-mat] (2008).

[3] P.W. Anderson, Science **316,** 1705 (2007).

[4] K-Y. Yang et al., arXiv:0810.3045 [cond-mat] (2008).

[5] Y. Kohsaka et al., Nature **454**, 1072 (2008).

[6] Y. Kohsaka et al., Science **315**, 1380 (2007).

[7] D.J. Pringle, G.V.M. Williams , and J.L. Tallon, Phys. Rev. B **62**, 12527 (2000).

[8] D. Zech et al., Nature **371**, 681 (1994).

[9] K.C. Hewitt et al., Phys. Rev. B **69**, 064514 (2004).

[10] L. Pintschovius, Phys. Status Solidi (b) **242** 30 (2005).

[11] F. Giustino, M. L. Cohen, and S. G. Louie, Nature **452**, 975 (2008).

[12] R. Heid et al., Phys. Rev. Lett. **100**, 137001 (2008).

[13] D.M. Newns and C.C. Tsuei, Nature Physic*s* **3**, 184 (2007).

[14] A. Bussman-Holder and A.R. Bishop, Phys. Rev. B **44**, 2853 (1991).

[15] V.H. Crespi, and M.L. Cohen, Phys. Rev. B **48**, 398 (1993).

[16] G.D. Mahan, Phys. Rev. B **56**, 8322 (1997).

[17] C. C. Tsuei and J. R. Kirtley, Rev. Mod. Phys. **72**, 969 (2000).

[18] R. Car and M. Parrinello, Phys. Rev. Lett. **55**, 2471 (1985).

[19] A. Bianconi et al., Phys. Rev. Lett. **76**, 3412 (1996).

[20] W.E. Pickett, R.E. Cohen, and H. Krakauer, Phys. Rev. Lett. **67**, 228 (1991).

[21] E. Pavarini et al., Phys. Rev. Lett. **87**, 047003 (2001).

[22] R.S. Markiewicz, J. Phys. Chem. Solids **58**, 1179 (1997).

[23] M. Le Tacon et al., Nature Physics **2**, 537 (2006).

[24] A.G. Loeser et al., Science **273**, 325 (1996).

[25] H. Ding et al., Nature **382**, 51 (1996).

[26] Jinho Lee et al., Nature **442**, 546 (2006).

[27] M. R. Norman et al., Phys. Rev. B **76**, 174501 (2007); M. R. Norman et al., Nature **392**, 157 (1998).

[28] A. Kanigel et al., Nature Physics **2**, 447-451 (2006).

arXiv:0902.3015v1 [cond-mat.supr-con] 17 Feb 2009

Giant Nonlinear Electron-lattice Interaction in Cuprate Superconductors, and Origin of the Pseudogap

R. Nistor[2], G.J. Martyna[1], M. H. Müser[1,2], D.M. Newns[1]and C.C. Tsuei [1]

[1]*IBM T.J. Watson Research Center,*

Yorktown Heights, NY 10598, USA and

[2]*Dept. of Applied Mathematics, University of Western Ontario,*

London, Ontario, Canada N6A 5B7

I. *AB INITIO* MOLECULAR DYNAMICS

The Car-Parrinello ab initio MD [1] studies presented herein were performed using Kohn-Sham Density Functional Theory. The CPMD approach is based on the Born-Oppenheimer approximation. It describes the metallic state, but not the magnetic, insulating state, of the cuprate materials. The computations were checked by comparison with the band structures of copper and the 214 material [2]. The Fig. 1 results were obtained by starting with the Fig. 1a configuration and running to equilibrium. The Fig. 2b results were obtained by constraining the oxygens in the manner shown in Fig. 1a at a specified value of the oxygen displacement, and running to equilibrium - they therefore represent "ion-relaxed" potential energy curves. Doping was achieved by varying the K/Ca ratio in the ensemble. Samples of 4x4 and 6x6 unit cells were run in periodic boundary conditions.

II. PROJECTION OF 3-BAND MODEL ONTO 1-BAND MODEL

In matrix notation consider a d-subspace and a p-subspace, represented by the Hamiltonians H^d and H^p respectively, connected by the coupling matrix V^{pd}, the Hamiltonian then being

$$H = \begin{bmatrix} H^d & V^{dp} \\ V^{pd} & H^p \end{bmatrix}. \tag{1}$$

Projecting onto the d-subspace in perturbation theory

$$\widetilde{H^d} = H^d + V^{dp}\left(\epsilon_d - H^p\right)^{-1} V^{pd}. \tag{2}$$

if i, j are d-sites, and l, m are p-orbitals

$$\widetilde{H^d}_{ij} = \epsilon_d \delta_{ij} + \sum_{l,m} V^{dp}_{il} \left(\epsilon_d - H^p\right)^{-1}_{lm} V^{pd}_{mj}. \tag{3}$$

Now we shall neglect the pp hopping matrix elements (Emery model), when $l = m$ and the V's are nearest-neighbor hopping matrix elements defined as $t_{pd} > 0$ (see Fig. 1). There are 2 processes,

1. i, j nearest neighbor $\langle i, j \rangle$ on the d-lattice, when the 2 V's have opposite sign (Fig. 1)

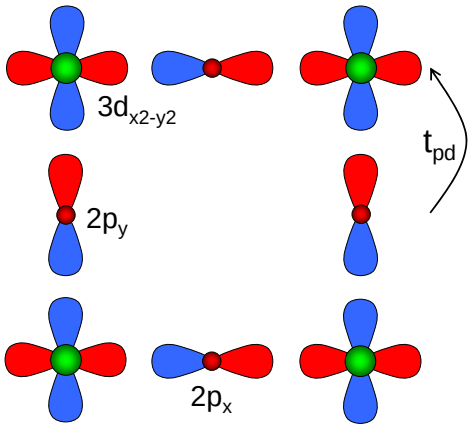

FIG. 1: $2p_x$, $2p_y$ and $3d_{x^2-y^2}$ orbitals in CuO_2 plane, illustrating $2p$ to $3d$ hopping integral t_{pd}.

2. $i = j$, when the 2 V's have same sign

giving

$$\widetilde{H^d} = \sum_{i,\sigma} \epsilon_d n_{i\sigma} + \sum_{\langle i,j\rangle,\sigma} \frac{t_{p_{ij}d}^2}{\epsilon_{p_{ij}d}} \left(n_{i\sigma} + n_{j\sigma}\right) - \sum_{\langle i,j\rangle} \frac{t_{p_{ij}d}^2}{\epsilon_{p_{ij}d}} X_{ij}, \tag{4}$$

where $\epsilon_{pd} = \epsilon_d - \epsilon_p > 0$ is the "oxide gap" between the oxygen $2p$ orbital energy and the higher-lying Cu $3d_{x^2-y^2}$ orbital energy, σ is spin, p_{ij} is the p-orbital between d-sites i and j, and the bond order operator X_{ij} is

$$X_{ij} = \sum_{\sigma} \left(c_{i\sigma}^{+} c_{j\sigma} + c_{j\sigma}^{+} c_{i\sigma}\right). \tag{5}$$

Let us assume that the oxygen motion in some direction is x, and that it enters the 3-band hamiltonian via the pd hopping integral

$$t_{pd} \to t_{pd} - v_{pd} x^2, \quad \text{where } v_{pd} > 0, \tag{6}$$

then to order v_{pd}, and defining $t = t_{pd}^2/\epsilon_{pd}$

$$\begin{aligned} \widetilde{H^d} = {} & (\epsilon_d + 2t) \sum_{i,\sigma} n_{i\sigma} - t \sum_{\langle i,j\rangle} X_{ij} \\ & - \frac{2t_{pd} v_{pd}}{\epsilon_{pd}} \sum_{\langle i,j\rangle,\sigma} \left(n_{i\sigma} + n_{j\sigma}\right) x_{ij}^2 + \frac{2t_{pd} v_{pd}}{\epsilon_{pd}} \sum_{\langle i,j\rangle} X_{ij} x_{ij}^2. \end{aligned} \tag{7}$$

Restoring our original notation [3] $2t_{pd}v_{pd}/\epsilon_{pd} = v/2\sqrt{nn_s}$, when the coupling v is seen to be **positive**

$$\widetilde{H^d} = (\epsilon_d + 2t)\sum_{i,\sigma} n_{i\sigma} - t\sum_{\langle i,j\rangle} X_{ij} \tag{8}$$
$$- \frac{v}{2\sqrt{nn_s}}\sum_{\langle i,j\rangle,\sigma}(n_{i\sigma} + n_{j\sigma})\, x_{ij}^2 + \frac{v}{2\sqrt{nn_s}}\sum_{\langle i,j\rangle} X_{ij}x_{ij}^2.$$

We retrieve our previous 1-band model (next-nearest and next-next-nearest neighbor hoppings are dropped due to neglect of t_{pp}), but with an extra term diagonal in d-space. As regards the vibrator, the effect of the new term is to weaken the oxygen parabolic potential linearly with increasing electron occupation of the band (or stiffen the vibrator with increasing hole occupation). The number operator term is dominant over the hopping term (<X> maximizes at $\simeq 0.6$).

Let us now alternatively assume that the oxygen motion enters the 3-band hamiltonian through the interaction of the electrostatic potential with the charge on the oxygen

$$\epsilon_{pd} \rightarrow \epsilon_{pd} + v_p x^2; \tag{9}$$

where v_p depends on a Madelung sum. In an ionic crystal it is arguable that the sign of v_p will be positive since the environment of a negative ion typically consists of positive ions, so as the O-ion approaches them the local oxide gap ϵ_{pd} becomes larger. However in a perovskite structure the issue needs specific calculation.

Expanding to first order

$$\frac{1}{\epsilon_{pd} + v_p x^2} = \frac{1}{\epsilon_{pd}} - \frac{v_p x^2}{\epsilon_{pd}^2}. \tag{10}$$

Returning to Eq. (4), we insert the foregoing expansion into the 2 terms to obtain

$$\Delta\widetilde{H^d} \rightarrow -\frac{tv_p}{\epsilon_{pd}}\sum_{\langle i,j\rangle}(n_{i\sigma} + n_{j\sigma})\, x_{ij}^2 + \frac{tv_p}{\epsilon_{pd}}\sum_{\langle i,j\rangle} X_{ij}x_{ij}^2. \tag{11}$$

The effect of the oscillator correction (11) from this mechanism can be absorbed into (8), giving the same final result (8) but with

$$\frac{v}{2\sqrt{nn_s}} = (2t_{pd}v_{pd} + tv_p)\,/\epsilon_{pd}. \tag{12}$$

The sign of v will be positive if the $t_{pd}v_{pd}$ term in parenthesis is dominant, or if v_p is positive as argued above.

In this section we have formally derived the FBM coupling, showing the approximations involved explicitly, and demonstrated the existence of a new term in the coupling.

III. FBM HAMILTONIAN

The FBM Hamiltonian involves three pieces

$$H = H^v + H^e + H^{ev}. \tag{13}$$

In H the Cu sites, which define the unit cell, are defined as 2D integral-component vectors $\mathbf{i} = (i_x, i_y)$ (lattice constant is taken as unity). The two oxygens in each unit cell $\mathbf{i}$ are located at the sites $\mathbf{i}+\widehat{\alpha}/2$, where $\widehat{\alpha}$ is a unit vector along the x- or y- axes, hence $\widehat{\alpha}$ defines whether the oxygen is in a Cu-O-Cu bond oriented along the x- or y- direction.

In the vibrator piece H^v the oxygen degree of freedom is an n-component vector $\mathbf{x}_{\mathbf{i}+\widehat{\alpha}/2}$, where $n = 1$ if a single mode is dominant (as assumed in the manuscript), $n = 2$ if the two modes transverse to the Cu-O-Cu bond are roughly equivalent, or in a case now considered unlikely (as the along-bond mode is found to be weakly coupled) $n = 3$ if the two transverse modes and the along-bond mode can all be considered equivalent. H^v is given by

$$H^v = \sum_{\mathbf{i},\alpha=\mathbf{x}}^{\mathbf{y}} \left[\frac{1}{2m} p^2_{\mathbf{i}+\widehat{\alpha}/2} + \frac{\chi_0}{2} x^2_{\mathbf{i}+\widehat{\alpha}/2} + \frac{w}{8n} \left(x^2_{\mathbf{i}+\widehat{\alpha}/2} \right)^2 \right]. \tag{14}$$

In H^v the scalar products $\mathbf{x}_{\mathbf{i}+\widehat{\alpha}/2} \cdot \mathbf{x}_{\mathbf{i}+\widehat{\alpha}/2}$ are abbreviated to $x^2_{\mathbf{i}+\widehat{\alpha}/2}$, and a momentum $\mathbf{p}_{\mathbf{i}+\widehat{\alpha}/2}$ conjugate to coordinate $\mathbf{x}_{\mathbf{i}+\widehat{\alpha}/2}$ is introduced, to define the vibrator kinetic energy, with m the oxygen mass (M in the Ms.). The "bare" bond force constant is χ_0. The quartic term, with coefficient w, is assumed in the degenerate case to be radially ($n = 2$) or spherically ($n = 3$) symmetric.

The electronic piece H^e is

$$H^e = -\frac{1}{2} \sum_{\mathbf{i},\mathbf{j},\sigma} t\,(\mathbf{i}-\mathbf{j})\, c^+_{\mathbf{i},\sigma} c_{\mathbf{j},\sigma}, \tag{15}$$

where $c^+_{\mathbf{i},\sigma}(c_{\mathbf{i},\sigma})$ denote respectively the creation (destruction) operators for the $3d_{x^2-y^2}$ orbital (or, more rigorously, the $d_{x^2-y^2}$-type Cu3d-O2p antibonding Wannier function) on lattice site $\mathbf{i}$ of spin σ. The strongest interaction is the nearest neighbor hopping integral $t(\pm 1, 0) = t(0, \pm 1) = t$, ($t$ is positive), followed by the next-nearest neighbor interaction $t(\pm 1, \pm 1) = t'$, (t' is negative) and then the 3rd-nearest neighbor interaction $t(\pm 2, 0) = t(0, \pm 2) = t''$ (t'' is positive). The band eigenvalues $\epsilon_{\mathbf{k}}$ of (15) are

$$\epsilon_{\mathbf{k}} = -2t(\cos k_x + \cos k_y) - 4t' \cos k_x \cos k_y - 2t''(\cos 2k_x + \cos 2k_y). \tag{16}$$

The model band structure has a minimum at Γ ($\mathbf{k} = (0,0)$), a maximum at Z ($\mathbf{k} = (\pi,\pi)$), and saddle points (SP) at X ($\mathbf{k} = (0,\pi)$), and Y ($\mathbf{k} = (\pi,0)$). As a result of the saddle points, located at $\epsilon_{\mathbf{SP}} = 4t' - 4t''$, the density of states (DOS) has a logarithmic peak (van Hove singularity or vHs) at $\epsilon_{\mathbf{SP}}$ which is found from ARPES and band structure calculations for near-optimally doped systems to lie close to the Fermi level [4, 5] - the resulting high DOS at the Fermi level strongly enhances the FBM coupling. The total band width is $8t$.

The electron-vibrator coupling piece is

$$H^{ev} = \frac{v}{2\sqrt{nn_s}} \sum_{\mathbf{i},\alpha=\mathbf{x}}^{\mathbf{y}} x^2_{\mathbf{i}+\widehat{\alpha}/2} \left[-\sum_{\sigma} \left(n_{\mathbf{i},\sigma} + n_{\mathbf{i}+\widehat{\alpha},\sigma} \right) + X_{\mathbf{i}+\widehat{\alpha}/2} \right]; \tag{17}$$

$$X_{\mathbf{i}+\widehat{\alpha}/2} = \sum_{\sigma} \left(c^+_{\mathbf{i},\sigma} c_{\mathbf{i}+\widehat{\alpha},\sigma} + c^+_{\mathbf{i}+\widehat{\alpha},\sigma} c_{\mathbf{i},\sigma} \right), \tag{18}$$

where the bond order operator X is associated with the oxygen site at the bond center, and we have defined in the mixed degeneracy factor $(nn_s)^{-1/2}$, where $n_s = 2$ is the spin degeneracy, to make the term of order $\sqrt{nn_s}$, motivated by a version of large-N theory jointly expanding in $1/n$ and $1/n_s$. In Ref. [3] only the X-piece of (17) was included.

The combination $-\sum_\sigma \left(n_{\mathbf{i},\sigma} + n_{\mathbf{i}+\widehat{\alpha},\sigma} \right) + X_{\mathbf{i}+\widehat{\alpha}/2}$ can also be written in more compact form, defining the antibonding orbital $|a, \mathbf{i}+\widehat{\alpha}/2\rangle = \left(|\mathbf{i}\rangle - |\mathbf{i}+\widehat{\alpha}\rangle \right)/\sqrt{2}$, with number operator $n^a_{\mathbf{i}+\widehat{\alpha}/2}$ (summing over spin). In the manuscript n^a is simplified to N.

$$-\sum_{\sigma} \left(n_{\mathbf{i},\sigma} + n_{\mathbf{i}+\widehat{\alpha},\sigma} \right) + X_{\mathbf{i}+\widehat{\alpha}/2} = -2n^a_{\mathbf{i}+\widehat{\alpha}/2}. \tag{19}$$

The complete Hamiltonian $H = H^v + H^e + H^{ev}$ is then

$$H = \sum_{\mathbf{i},\alpha=\mathbf{x}}^{\mathbf{y}} \left[\frac{1}{2m} p^2_{\mathbf{i}+\widehat{\alpha}/2} + \frac{\chi_0}{2} x^2_{\mathbf{i}+\widehat{\alpha}/2} + \frac{w}{8n} \left(x^2_{\mathbf{i}+\widehat{\alpha}/2} \right)^2 \right] - \frac{1}{2} \sum_{\mathbf{i},\mathbf{j},\sigma} t\left(\mathbf{i}-\mathbf{j}\right) c^+_{\mathbf{i},\sigma} c_{\mathbf{j},\sigma} \tag{20}$$
$$+ \frac{v}{\sqrt{nn_s}} \sum_{\mathbf{i},\alpha=\mathbf{x}}^{\mathbf{y}} x^2_{\mathbf{i}+\widehat{\alpha}/2} n^a_{\mathbf{i}+\widehat{\alpha}/2}.$$

Note that in Eq.(20) $K = v^2/w$ defines a coupling energy.

IV. DETERMINATION OF COUPLING v

Calculation of the oxygen PE surface as a function of doping is not an ideal approach to calculationg the FBM coupling constant for two reasons. The PE surface calculations such as illustrated in Fig. 2 in the Ms. are relaxed surfaces, i.e. when certain oxygen coordinates

are held fixed all other atoms are allowed to find their minumum energy. This differs from the "vertical" couplings entering the FBM Hamiltonian, where atoms other than planar oxygen are assumed fixed in place. Secondly the coupling in the FBM Hamiltonian is to the number of electrons n^a in the antibonding orbital, which mainly involves states at the top of the d-band and will be filled mainly by adding electrons rather than holes as was done (for reasons of computational stability) in Fig. 2 of the Ms..

The method adopted to calculate the coupling strength v is based on comparing the shift in band structure energies when the oxygen location is perturbed with the same shift deduced from the FBM Hamiltonian. The FBM coupling (third term in Eq.(20)) leads to splittings in the tight-binding band structure. If all oxygens in the x-oriented bonds are globally shifted by u_x, and all oxygens in the y-oriented bonds by u_y, there is a splitting of the band energy between the band energy ϵ_X at the saddle point (SP) X= $(\pi, 0)$, and ϵ_Y at Y= $(0, \pi)$, given by $\epsilon_X - \epsilon_Y = \sqrt{2/n}v\left(u_x^2 - u_y^2\right)$. By numerically calculating the band structure with first the x-oxygens displaced, and then the y-oxygens, and subtracting the corresponding band structure energies energies at, say, the SP X, any isotropic shift resulting from displacing a single oxygen can be cancelled out and the coupling v determined. The results are shown in Table I.

V. MEAN FIELD APPROXIMATION

Mean field theory is a useful step in investigating the properties of many models. In the FBM, the mean field approximation decouples the electronic and vibrational parts of the Hamiltonian. In the vibrational part, an expectation value of the electronic terms shifts the oscillator harmonic frequency, the expectation value being assumed spatially uniform, but it can be different in the x- and y- bonds (in this section we return to the notation in the Ms.):

$$H^{vib} = \sum_{\langle i,j\rangle} \frac{p_{ij}^2}{2M} + \frac{1}{2}\sum_{\langle i,j\rangle} \chi_0 u_{ij}^2 + \frac{w}{8}\sum_{\langle i,j\rangle} u_{ij}^4 + \frac{v}{2\sqrt{2}}\sum_{\langle i,j\rangle,\sigma} \left(2 - 2p + \left\langle c_{i,\sigma}^+ c_{j,\sigma} + c_{j,\sigma}^+ c_{i,\sigma}\right\rangle\right) u_{ij}^2. \tag{21}$$

H^{vib} can easily be diagonalized in a harmonic oscillator basis. In the electronic part, the expectation value of the square of the oscillator amplitude has been taken,

$$H^{el} = \sum_{\mathbf{k},\sigma} \epsilon_{\mathbf{k}} n_{\mathbf{k},\sigma} + \frac{v}{2\sqrt{2}} \sum_{\langle i,j\rangle,\sigma} \left[c^{+}_{i,\sigma} c_{j,\sigma} + c^{+}_{j,\sigma} c_{i,\sigma} \right] \left\langle u^2_{ij} \right\rangle , \tag{22}$$

giving a band structure problem in which there are new nearest-neighbor hopping terms $\left(v/2\sqrt{2}\right) \left[c^{+}_{i,\sigma} c_{j,\sigma} + c^{+}_{j,\sigma} c_{i,\sigma} \right] \left\langle u^2_{ij} \right\rangle$ (the uniform shift represented by the number operator terms does not change the band structure and is omitted) with the effect of reducing the nearest-neighbor hopping integral. Allowing the oscillator amplitude squared for the x-directed $\left\langle u^2_{ij} \right\rangle_x$ and y-directed $\left\langle u^2_{ij} \right\rangle_y$ bonds to be unequal (the C4 symmetry-split case), the band structure is changed to

$$\widetilde{\epsilon}_{\mathbf{k}} = \epsilon_{\mathbf{k}} + \frac{v}{\sqrt{2}} \left\langle u^2_{ij} \right\rangle_x \cos k_x + \frac{v}{\sqrt{2}} \left\langle u^2_{ij} \right\rangle_y \cos k_y . \tag{23}$$

Using the band structure $\widetilde{\epsilon}_{\mathbf{k}}$ (23) the expectation values $\left\langle c^{+}_{i,\sigma} c_{j,\sigma} + c^{+}_{j,\sigma} c_{i,\sigma} \right\rangle$ for x-oriented and y-oriented bonds are calculated, hence defining two quartic Hamiltonians (21) whose exact solution yields the squared vibrator amplitudes $\left\langle u^2_{ij} \right\rangle_x$ and $\left\langle u^2_{ij} \right\rangle_y$. These interconnected electronic and quartic problems are then solved self-consistently as regards the expectation values. The parameters used were similar to Table I, $v = 0.0198$ au, $w = 0.085$ au, the oscillator bare force constant was $\chi_0 = -0.0225$ au. The band structure is parametrized by the (negative of the) hopping matrix elements, the nearest-neighbor hopping matrix element $t = 0.25$ eV, next-nearest-neighbor hopping m.e. $t' = -0.05$ eV, and third next-nearest-neighbor hopping m.e. $t'' = 27.2$ meV.

We can rewrite the effective band structure as

$$\widetilde{\epsilon}_{\mathbf{k}} = \overline{\epsilon_{\mathbf{k}}} + \frac{1}{2} \Delta_{ps} \left(\cos k_x - \cos k_y \right) , \tag{24}$$

where $\Delta_{ps} = \left(v/\sqrt{2}\right) \left(\left\langle u^2_{ij} \right\rangle_x - \left\langle u^2_{ij} \right\rangle_y \right)$ is the pseudogap, and the renormalized nearest-neighbor hopping $\left(v/2\sqrt{2}\right) \left(\left\langle u^2_{ij} \right\rangle_x + \left\langle u^2_{ij} \right\rangle_y \right)$ is absorbed into $\overline{\epsilon_{\mathbf{k}}}$. The experimental data [6] show that the pseudogap is not uniform over the sample as we have, for simplicity, assumed, but the coherence length over which the sign of Δ^0_{ps} varies is quite short, only a few lattice spacings. Probably as a result of this nanoscopic domain structure, the phase boundary of the pseudogap region is not typically found experimentally to constitute a true, sharp, phase boundary [7].

The variation of pseudogap with doping at low temperature seen in the contour plot (Manuscript Fig. 3) is similar to thet seen in experimental data [8] (see Fig. 2)

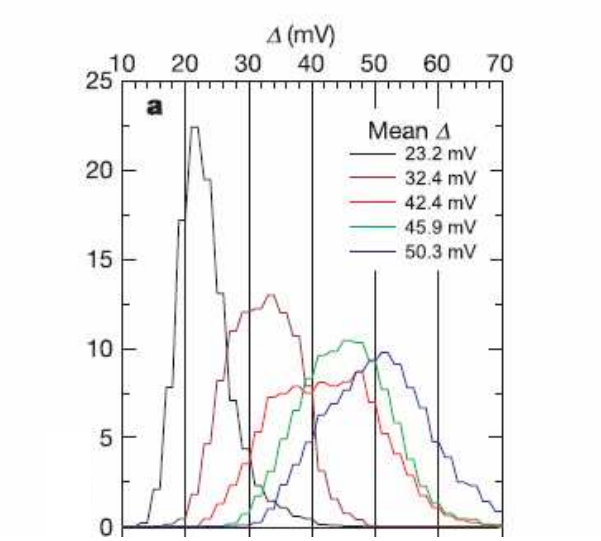

Histograms of measured energy gaps Δ from a sequence of samples with different dopings, black being strongly overdoped and blue strongly underdoped.

FIG. 2: Histograms of measured energy gaps Δ from a sequence of samples with different dopings, black being strongly overdoped and blue strongly underdoped [8].

VI. INTENSITY VARIATION IN EXPERIMENTAL R-PLOTS

In order to model the experimental behavior in the STM experiments [6] on C4 symmetry-split systems, we calculated the projected DOS for a 3-band model with the basis of oxygen $2p_x$ and $2p_y$ orbitals and Cu $3d_{x^2-y^2}$ orbitals shown in Fig. 1. The $pd\sigma$ hopping matrix element is $t_{pd} = 1.12$ eV. There are pp hopping matrix elements between nearest-neighbor $2p_x$ and $2p_y$ orbitals given by $t_{pp} = -0.528$ eV, and an oxide gap $\epsilon_d - \epsilon_p = 6$ eV. A spatially-uniform pseudogap is introduced by modifying the t_{pd} matrix elements to $t_{p_x d} = t_{pd} + \Delta t$ (i.e. for the lower vibrational amplitude oxygen) and $t_{p_y d} = t_{pd} - \Delta t$ (i.e. for the higher vibrational amplitude oxygen), where $\Delta t = 0.0375$ eV (the argument below only depends on these being semiquantitatively correct). The results for the DOS projected into the oxygen $2p_x$ orbitals (lying in x-oriented Cu-O-Cu bonds - see Fig. 1) and oxygen $2p_y$ orbitals are different, as seen in Fig. 3. The DOS peak associated with the van Hove singularity is seen in Fig. 3 to be split, the peak above the Fermi level being localized only on the lower vibrational amplitude oxygen, and the peak below the Fermi level being being localized only the higher vibrational amplitude oxygen. The STM R-map technique [6] for detecting the C4 splitting experimentally involves the ratio R of the tunneling current into the empty DOS to the hole current into the filled DOS. Evidently from Fig3 , R is predicted to be large on

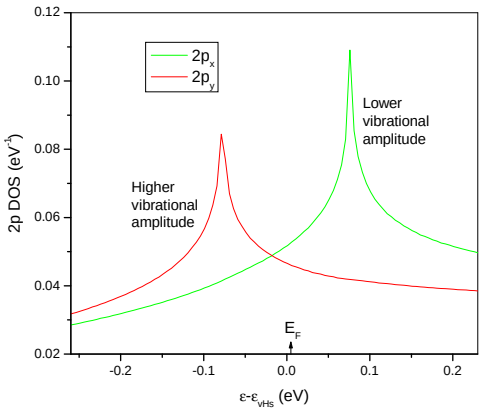

FIG. 3: Oxygen projected $2p$-DOS for oxygens in x-oriented and y-oriented bonds.The peak above the Fermi level is for the lower vibrational amplitude oxygen, and the peak below the Fermi level is for the higher vibrational amplitude oxygen.

the low amplitude oxygens and small on the high amplitude oxygens, in agreement with the observation [6], in which the high amplitude oxygens are associated with dark streaks in the R-map, while the low amplitude oxygens are associated with bright spots. Note that the C4 splitting is characterized by nanoscale domains [6].

VII. LAGRANGIAN FORMALISM

Here we wish to derive the pairing interaction in the FBM. For this purpose a simple approach, akin to the familiar RPA, is to utilise the $1/N$ expansion technique, where N is degeneracy, e.g. vibrational degeneracy n or spin degeneracy n_s. In this approach the exact solution to the $n = 1$ quartic vibrator used in the main Ms. will be replaced by the (very similar) mean field solution to the $n > 1$ quartic vibrator [3]. The $1/N$ expansion works well e.g. for the Kondo problem [9], the results remaining physical down to spin degeneracy $n_s = 2$. Here we symetrically co-expand in the inverse of the mode degeneracy n and the spin degeneracy n_s [10], meaning by expressions such as "$1/N$" the joint orders $1/n$ and $1/n_s$. The $1/N$ expansion technique is usually implemented within a Lagrangian/path integral formulation [10], the approach we shall adopt here. We take $\hbar = 1$, and omit the

sum-normalizing factors $1/N_x^2$, which can always be restored by inspection.

Within the usual imaginary time (Euclidean) Lagrangian formulation at finite temperature the partition function can be written

$$Z = \int \mathcal{D}x\mathcal{D}c e^{-\int_0^\beta \mathcal{L}(\tau)d\tau}, \tag{25}$$

where $\mathcal{L}(\tau)$ is the Lagrangian as a function of imaginary time τ, β is $1/T$ (T is temperature, taking Boltzmann's constant $k_B = 1$), $\int \mathcal{D}x\mathcal{D}c$ implies a path integral over the vibrator and fermionic (Grassman) variables.

The Lagrangian, readily derived from the Hamiltonian (20),

$$\mathcal{L} = \mathcal{L}_e^{(1)} + \mathcal{L}_v^{(1)} + \mathcal{L}_v^{(2)} + \mathcal{L}_{ev}^{(2)}, \tag{26}$$

comprises the previously described terms (15), (14), and (17)

$$\begin{aligned}
\mathcal{L}_e^{(1)} &= \sum_{\mathbf{i},\sigma} c_{\mathbf{i},\sigma}^+ \frac{\partial}{\partial\tau} c_{\mathbf{i},\sigma} - \frac{1}{2}\sum_{\mathbf{i},\mathbf{j},\sigma} t\left(\mathbf{i}-\mathbf{j}\right) c_{\mathbf{i},\sigma}^+ c_{\mathbf{j},\sigma}, . \\
\mathcal{L}_v^{(1)} &= \frac{1}{2}\sum_{\mathbf{i},\alpha}\left[m\dot{x}_{\mathbf{i}+\widehat{\alpha}/2}^2 + \chi_0 x_{\mathbf{i}+\widehat{\alpha}/2}^2\right], \\
\mathcal{L}_v^{(2)} &= \frac{w}{8n}\sum_{\mathbf{i},\alpha}\left(x_{\mathbf{i}+\widehat{\alpha}/2}^2\right)^2, \\
\mathcal{L}_{ev}^{(2)} &= \frac{v}{\sqrt{nn_s}}\sum_{\mathbf{i},\alpha=\mathbf{x}}^{\mathbf{y}} x_{\mathbf{i}+\widehat{\alpha}/2}^2 n_{\mathbf{i}+\widehat{\alpha}/2}^a
\end{aligned} \tag{27}$$

A kinetic energy for the fermion variables is introduced on line 1, otherwise the terms are the same as in Eq's (15), (14), and (17). In the following we extend the earlier FBM results [3] to include the more complete form of coupling derived in Sec. II.

VIII. RESULTS

We implement a Stratonovic decoupling on the bilinear terms $\mathcal{L}_v^{(2)}$ and $\mathcal{L}_{ev}^{(2)}$ in the Lagrangian, generating path integrals over new fields $z_{v,\mathbf{i}+\widehat{\alpha}/\mathbf{2}}$ and $z_{e,\mathbf{i}+\widehat{\alpha}/\mathbf{2}}$ defined on each Cu-O-Cu bond. Later this will make it possible to implement the path integrals over the Boson and Fermion fields under the z-path integral.

Now the partition function is written in terms of the action S

$$Z = \int \mathcal{D}z\mathcal{D}x\mathcal{D}c e^{-\beta\mathcal{S}}, \tag{28}$$

which is again decomposed into the terms

$$S = S_v^{(1)} + S_e^{(1)} + S_z^{(2)} + S_{zv} + S_{ze}, \tag{29}$$

defined by

$$\begin{aligned}
S_v^{(1)} &= \frac{m}{2} \sum_{\mathbf{k},m,\alpha} \left(\omega_m^2 + \overline{\omega}_\alpha^2\right) x_{-\mathbf{k},-m,\alpha} x_{\mathbf{k},m,\alpha}, \\
S_e^{(1)} &= \sum_{\mathbf{k},m,\sigma} \left(\overline{\epsilon}_{\mathbf{k}} - i\nu_m\right) c^+_{\mathbf{k},m,\sigma} c_{\mathbf{k},m,\sigma}, \\
S_z^{(2)} &= \frac{n_s}{2K} \sum_{\mathbf{q},n,\alpha} z^e_{-\mathbf{q},-n,\alpha} z^e_{\mathbf{q},n,\alpha} - \frac{2\sqrt{nn_s}}{v} \sum_{\mathbf{q},\alpha,n} z^e_{-\mathbf{q},-n,\alpha} z^v_{\mathbf{q},n,\alpha}, \\
S_{zv} &= -\sum_{\mathbf{q},\mathbf{k},n,m,\alpha} z^v_{-\mathbf{q},-n,\alpha} x_{-\mathbf{k},-m,\alpha} x_{\mathbf{k}+\mathbf{q},m+n,\alpha} + \sum_\alpha z^v_{\mathbf{0},0,\alpha} \left\langle x^2 \right\rangle, \\
S_{ze} &= \sum_{\mathbf{q},n,\sigma,\alpha} \psi^\alpha_{\mathbf{k},\mathbf{k}+\mathbf{q}} z^e_{-\mathbf{q},-n,\alpha} c^+_{\mathbf{k},m,\sigma} c_{\mathbf{k}+\mathbf{q},m+n,\sigma} - 2\sum_\alpha z^e_{\mathbf{0},0,\alpha} \left\langle n^a \right\rangle.
\end{aligned} \tag{30}$$

Here

$$\begin{aligned}
x(t) &= \sum_n e^{-i\omega_n t} x_n, \quad \omega_n = 2n\pi T; \qquad \text{Bose and z fields,} \\
c(t) &= \sum_n e^{-i\nu_n t} c_n, \quad \nu_n = (2n+1)\,\pi T; \quad \text{Fermion fields,}
\end{aligned} \tag{31}$$

define the Fourier series converting to Bosonic and Fermionic Matsubara frequencies ω_n and ν_n, and a coupling amplitude $\psi^\alpha_{\mathbf{k},\mathbf{k}'}$ different from that in [3] appears

$$\psi^\alpha_{\mathbf{k},\mathbf{k}'} = 4\sin\left[k_\alpha/2\right] \sin\left[k'_\alpha/2\right]. \tag{32}$$

The band structure $\overline{\epsilon}_{\mathbf{k}}$ and vibrator frequencies $\overline{\omega}_\alpha$ now involve mean field quantities, an effective nearest-neighbor hopping integral t_α (33) defined by

$$t_\alpha = t + z_e^\alpha = t - \frac{v}{2\sqrt{nn_s}} \left\langle x^2 \right\rangle_\alpha, \tag{33}$$

physically meaning that the effective hopping is weakened by the vibrational displacement of the oxygen, and vibration frequencies $\overline{\omega}_\alpha$ given by (34)

$$\begin{aligned}
m\overline{\omega}_\alpha^2 &= \chi_0 - 2z_v^\alpha \\
&= \chi_0 - \frac{2v}{\sqrt{nn_s}} \left\langle n^a \right\rangle_\alpha + \frac{w}{2n} \left\langle x^2 \right\rangle_\alpha.
\end{aligned} \tag{34}$$

physically meaning that the quasiharmonic vibrator is softened by the number of antibonding electrons $\langle n^a \rangle_\alpha$, and stiffened by the effect of the quartic potential.

On implementing the path integrals over the Boson and Fermion fields under the z-path integral (here we drop the α-dependence of the mean field quantities for simplicity), we obtain to order $(1/N)$ the quasi-harmonic action

$$S = \frac{1}{2} \sum_{\mathbf{q},n} \left[z^v_{-\mathbf{q},-n,x}, z^v_{-\mathbf{q},-n,y} z^e_{-\mathbf{q},-n,x}, z^e_{-\mathbf{q},-n,y} \right] \mathbf{A}(\mathbf{q},n) \begin{bmatrix} z^v_{\mathbf{q},n,x} \\ z^v_{\mathbf{q},n,y} \\ z^e_{\mathbf{q},n,x} \\ z^e_{\mathbf{q},n,y} \end{bmatrix}, \tag{35}$$

where the matrix $\mathbf{A}$ is given by

$$\mathbf{A}(\mathbf{q},n) = \begin{bmatrix} -nD_2(n) & 0 & -\frac{2\sqrt{nn_s}}{v} & 0 \\ 0 & -nD_2(n) & 0 & -\frac{2\sqrt{nn_s}}{v} \\ -\frac{2\sqrt{nn_s}}{v} & 0 & \frac{n_s}{K}\left(1 - KR_{xx}(\mathbf{q},n)\right) & -n_s R_{xy}(\mathbf{q},n) \\ 0 & -\frac{2\sqrt{nn_s}}{v} & -n_s R_{yx}(\mathbf{q},n) & \frac{n_s}{K}\left(1 - KR_{yy}(\mathbf{q},n)\right) \end{bmatrix}, \tag{36}$$

and the Response functions (RF) are defined by

$$D_2(\mathbf{q},n) = \frac{2}{m^2 \overline{\omega}} \left[\frac{1}{(\omega_n^2 + 4\overline{\omega}^2)} \coth\left(\frac{\overline{\omega}}{2T}\right) + \frac{\delta_{n,0}}{8T\overline{\omega} \sinh^2\left(\frac{\overline{\omega}}{2T}\right)} \right], \tag{37}$$

and ($f(\epsilon)$ is the Fermi function)

$$R_{\alpha\beta}(\mathbf{q},n) = -\sum_{\mathbf{k}} \frac{f(\epsilon_{\mathbf{k}}) - f(\epsilon_{\mathbf{k}+\mathbf{q}})}{\epsilon_{\mathbf{k}} - \epsilon_{\mathbf{k}+\mathbf{q}} + i\omega_n} \psi^\alpha_{\mathbf{k},\mathbf{k}+\mathbf{q}} \psi^\beta_{\mathbf{k}+\mathbf{q},\mathbf{k}}. \tag{38}$$

IX. DISCUSSION

The important regions of k-space in the Brillouin Zone are the high-density of states regions around the saddle points (SP) at $\mathbf{k} = (0,\pi)$ (termed Y), and $(\pi,0)$ (termed X). The key issue is to understand how the FBM behaves at the SP. Because of the ψ-factors, the RF are close to being diagonal if we assume only regions around the SP are important in the k-sum. Therefore the A-matrix separates into a component having a pole in the x-channel, and a component having a pole in the y-channel. At zero frequency and wavevector, these poles correspond to the onset of the phase boundary for the PG at T^*. As regards pairing, we consider the interaction for a pair to scatter from $(\mathbf{k},-\mathbf{k})$ to $(\mathbf{k}',-\mathbf{k}')$, which involves

the factor $\left(\psi^{\alpha}_{\mathbf{k},\mathbf{k}'}\right)^2$. This will either scatter where $\mathbf{k}$ and $\mathbf{k}'$ lie in the neighborhood of the point X which involves the factor $\left(\psi^{x}_{\mathbf{k},\mathbf{k}'}\right)^2 \sim 16$, in which case the inverse of the A-matrix in the x-channel is involved, or in the neighborhood of the point Y, which involves the factor $\left(\psi^{y}_{\mathbf{k},\mathbf{k}'}\right)^2 \sim 16$, in which case the inverse of the A-matrix in the y-channel is involved. The interaction has the classic form required for d-wave pairing, in that the interaction is attractive (in fact close to singular) for $(\mathbf{k}-\mathbf{k}')$ small, and at large $(\mathbf{k}-\mathbf{k}')$ the attraction dies off (in fact, because of the short-range repulsive interaction U, which is flat in k-space, the interaction actually becomes repulsive at large $(\mathbf{k}-\mathbf{k}')$).

The situation for the full FBM Hamiltonian (20) is similar but different in detail for the interaction which considers only the X-term in the electronic coupling (19) [3], when instead of the coupling amplitude $\psi^{\alpha}_{\mathbf{k},\mathbf{k}'}$ we have the amplitude

$$\chi^{\alpha}_{\mathbf{k},\mathbf{k}'} = -2\cos\left(\frac{k_\alpha + k'_\alpha}{2}\right). \tag{39}$$

This function leads to a different A-matrix [3], in which only a component with d-symmetry (the z's in the x- and y- channels having opposite sign) is singular, the other, s-channel, being nonsingular. Now scattering around either SP X or SP Y is possible with the the factor $\left(\chi^{\alpha}_{\mathbf{k},\mathbf{k}'}\right)^2 \sim 4$ for either $\alpha = x$ or $\alpha = y$. However only one combination of channels is singular, so we assume that this can be considered as if there is only one effective channel for scattering around each SP, just as in the case where both terms in the electronic coupling (19) are present. Hence we conclude on the basis of dominance by the SP, that the pairing interaction in the case of the full electronic coupling (19) is $4\times$ as large as that in the reduced interaction considered earlier. This is the result cited in the manuscript, which however needs verification by numerical solution of the gap equation.

---

[1] R. Car and M. Parrinello, Phys. Rev. Lett. **55**, 2471 (1985).

[2] Warren E. Pickett, Rev. Mod. Phys. **61**, 433 (1989).

[3] D.M. Newns and C.C. Tsuei, Nature Physics **3**, 184 (2007).

[4] E. Pavarini et al., Phys. Rev. Lett. **87**, 047003 (2001).

[5] X.J. Zhou et al. Phys. Rev. Lett. **92**, 187001 (2004).

[6] Y. Kohsaka et al., Science **315**, 1380 (2007).

[7] T. Timusk et al., Rep. Prog. Phys. **62,** 61 (1999).

[8] Jinho Lee et al., Nature **442**, 546 (2006).

[9] N. Read and D.M. Newns, J. Phys. C. **16**, 3273 (1983).

[10] Coleman, S., Aspects of Symmetry. Cambridge, New York, (1985).